A Complete Fault Diagnostic System for Automated Vehicles Operating in a Platoon

Rajesh Rajamani, *Member, IEEE*, Adam S. Howell, Chieh Chen, J. Karl Hedrick, and Masayoshi Tomizuka, *Fellow, IEEE*

***Abstract*—A "complete" fault diagnostic system is developed for automated vehicles operating as a platoon on an automated highway system. The diagnostic system is designed to monitor the complete set of sensors and actuators used by the lateral and longitudinal controllers of the vehicle, including radar sensors, magnetometers and inter-vehicle communication systems. A fault in any of the twelve sensors and three actuators is identified without requiring any additional hardware redundancy. The diagnostic system uses parity equations and several reduced-order nonlinear observers constructed from a simplified dynamic model of the vehicle. Nonlinear observer design techniques are used to guarantee asymptotically stable convergence of estimates for the nonlinear dynamic system. Different combinations of the observer estimates and the available sensor measurements are then processed to construct a bank of residues. The paper analytically shows that a fault in any one of the sensors or actuators creates a unique subset of these residues to grow so as to enable exact identification of the faulty component. Both simulation and experimental results are presented to demonstrate the effectiveness of the fault diagnostic system in the presence of various faults.**

***Index Terms*—Automated highway system, fault diagnostics, nonlinear observers, platoon, vehicle dynamics.**

NOMENCLATURE

x_i	Longitudinal position of the ith vehicle.
$\dot{x}_i$ or v_i or v	Longitudinal velocity of the ith vehicle.
$\varepsilon_i = x_i - x_{i-1} + L$	Longitudinal spacing error of the ith vehicle, with L being the desired spacing.
v_ℓ	Longitudinal velocity of the lead vehicle of the platoon.
$\ddot{x}_\ell$	Lngitudinal acceleration of the lead vehicle of the platoon.
T_{net}	Net combustion torque of the engine.
T_{br}	Brake torque.
ω_e	Engine angular speed.
c_a	Aerodynamic drag coefficient.
R	Gear ratio.
h	Tire radius.
F_f	Rolling resistance of the tires.
J_e	Effective inertia reflected on the engine side.
$\dot{m}_{ai}$	Rate of mass flow into engine manifold.
$\dot{m}_{a0}$	Rate of mass outflow from engine manifold.
$\dot{m}_a$	Rate of air mass flow in engine manifold.
P_m	Pressure of air in engine manifold.
y_{cg}	Lateral error at c.g. with respect to road.
$\Delta\varepsilon$	Vehicle yaw angle with respect to road.
$\Delta\dot{\varepsilon}$	Vehicle yaw rate with respect to road.
$\dot{\varepsilon}_d$	Yaw rate contribution of the road.
$C_{\alpha f}, C_{\alpha r}$	Front and rear cornering stiffness, respectively.
m	Vehicle mass.
δ	Seering angle.
ℓ_f, ℓ_r	Distances from c.g. to front tire and rear tire, respectively.

Manuscript received May 7, 1998. Manuscript received in final form February 7, 2001. Recommended by Associate Editor S. Farinwata.

R. Rajamani is with the Department of Mechanical Engineering, University of Minnesota, Minneapolis, MN 55455 USA.

A. Howell, J. K. Hedrick, and M. Tomizuka are with the Department of Mechanical Engineering, University of California, Berkeley, CA 94720 USA.

C. Chen is with the Department of Mechanical Engineering, National Chiao Tung University, Taiwan.

Publisher Item Identifier S 1063-6536(01)04930-2.

I. INTRODUCTION

THE Automated Highway Systems (AHS) Program at California PATH (Partners for Advanced Transit and Highways) aims to reduce congestion on highways by achieving significantly higher traffic flow through closer packing of automatically controlled vehicles into platoons. Studies of automatic control of the longitudinal and lateral motion of cars have been previously undertaken to establish feasibility of the AHS concept ([7], [11], [14]–[16] and [19]). These experimental studies have demonstrated the viability of automatic driver-less control of cars so as to achieve high traffic throughput on highways.

Studies have shown that over 90% of highway accidents occur due to driver-related errors. The AHS system eliminates these accidents by drastically reducing the burden of the driver. The reliability and safe operation of the hardware is, however, of increased importance. The present paper deals with this issue. It develops an automated health monitoring system for all the sensors and actuators used by the lateral and longitudinal controllers.

Classical results on the design of fault detection filters for linear time-invariant systems are available in White and Speyer [20]. Previous work on fault detection and fault tolerant control related to AHS have been carried out by Douglas *et al.* [4], Patwardhan and Tomizuka ([12], [13]) and Garg and Hedrick ([5], [6]).

The work of Douglas *et al.* [4] develops fault-detection filters for both longitudinal and lateral sensors using a linearized model of the vehicle dynamics. The model is linearized at the operating speed. The performance of the fault detection filters is then simulated using the original nonlinear vehicle models. Radar range and range rate, inter-vehicle communication, steering actuator and lateral magnetometer are not included

1063–6536/01$10.00 ©2001 IEEE

Authorized licensed use limited to: COLORADO STATE UNIVERSITY. Downloaded on April 16,2025 at 22:55:41 UTC from IEEE Xplore. Restrictions apply.

IPR2025-00943
Tesla EX1026 Page 1

among the sensors considered in the fault detection scheme. Fault detection filters for lateral control sensors have been developed by Patwardhan and Tomizuka [12] using linear time-invariant dynamic models linearized at the operating speed. Patwardhan and Tomizuka also design a parameter identification scheme using tire pressure measurements to detect and handle tire bursts [13]. The work by Garg and Hedrick ([5], [6]) utilizes results on the design of stable observers for nonlinear systems and enhances the observer design process to help in uniquely identifying sensor faults.

All of the above results successfully develop fault detection schemes that can identify faults in a small set of sensors and actuators on the vehicles, with the assumption that the other sensors do not have faults. The integration of the various fault detection schemes to provide a fault diagnostic system that can systematically monitor the health of all the sensors and actuators has not been addressed. Further, none of the results have developed fault detection filters that can identify faults in the radar, magnetometer, steering actuator and the communication system. The present paper addresses this issue. The contribution of the present paper is a complete fault diagnostic system for the entire control system hardware, including radar range and range rate, inter-vehicle communication radio, lateral magnetometer sensors and the steering actuator.

II. Simplified Model for Control Design

A. Simplified Longitudinal Vehicle Model

The reader is referred to Cho and Hedrick [2] and Hedrick, *et al.* [7] for a detailed model of the car's longitudinal dynamics. We present here the simplified model used very effectively for control design in [7].

Under the assumptions that there is no longitudinal slip between the tire and the road and that the torque converter is locked, the longitudinal velocity of the jth vehicle in the vehicle platooning scenario can be related to the angular velocity of the engine through the gear ratio and tire radius as follows:

$$\dot{x}_j = v_j = (Rh\omega_e)_j \tag{1}$$

where R is the gear ratio and h is the tire radius.

The dynamics relating engine speed ω_e to the pseudoinputs "net combustion torque" T_{net} and brake torque T_{br} and aerodynamic losses can be modeled by

$$\dot{\omega}_e = \frac{T_{\text{net}} - c_a R^3 h^3 \omega_e^2 - R(hF_f + T_{\text{br}})}{J_e} \tag{2}$$

where J_e is the effective inertia reflected on the engine side and is given by

$$J_e = I_e + (Mh^2 + I_\omega)R^2. \tag{3}$$

A description of all the variables and their symbols can be found in the Nomenclature section. The pseudoinput T_{net} is related to the throttle angle α (the actual control or actuator input) by the following dynamics. Steady-state engine maps define T_{net} as a nonlinear function of engine speed ω_e and the mass of air in the intake manifold $T_{\text{net}} = T_{\text{net}}(\omega_e, m_a)$. These steady-state maps are available for each car from the manufacturer and are obtained from standard dynamometer tests conducted after the engine has been designed and built.

The mass flow rate of air in the manifold is described by

$$\dot{m}_a = \dot{m}_{ai} - \dot{m}_{ao} \tag{4}$$

where $\dot{m}_{ai}$ is the inflow into the intake manifold and depends on the throttle angle α while $\dot{m}_{ao}$ is the mass flow rate into combustion chamber. The inflow can be described by

$$\dot{m}_{ai} = \text{MAX}\, TC(\alpha)\text{PRI}(m_a) \tag{5}$$

where MAX is a constant dependent on the size of the throttle body, $TC(\alpha)$ is a known nonlinear invertible function of the throttle angle and $\text{PRI}(m_a)$ is the pressure influence function which describes the choked flow relationship which occurs through the throttle valve. The outflow $\dot{m}_{ao}$ is a nonlinear function of P_m and ω_e and is available from the manufacturer in the form of a table.

B. Simplified Lateral Dynamics Model

A complete simulation model including a realistic representation of both the lateral and longitudinal dynamics is presented in Peng and Tomizuka [15]. A simplified lateral dynamics model incorporating only the lateral translation and yaw degrees of freedom is used for controller design and is available in [1], [15]. The simplified lateral dynamics model is derived by linearizing vehicle lateral dynamics with respect to the road centerline reference coordinates and is shown below

$$\dot{x} = Ax + B_1\delta + B_2\dot{\varepsilon}_d \tag{6}$$

with

$$x = \begin{Bmatrix} y_{\text{cg}} \\ \dot{y}_{\text{cg}} \\ \Delta\varepsilon \\ \Delta\dot{\varepsilon} \end{Bmatrix}, B_1 = \begin{Bmatrix} 0 \\ \frac{2C_{\alpha f}}{m} \\ 0 \\ \frac{2\ell_f C_{\alpha f}}{I} \end{Bmatrix}$$

$$B_2 = \begin{Bmatrix} 0 \\ \frac{-2}{mv}(\ell_f C_{\alpha f} - \ell_r C_{\alpha r}) \\ 0 \\ \frac{-2}{vI}\left({\ell_f}^2 C_{\alpha f} + {\ell_r}^2 C_{\alpha r}\right) \end{Bmatrix}$$

$$A = \begin{bmatrix} 0 & 1 & 0 & 0 \\ 0 & a_{22} & a_{23} & a_{24} \\ 0 & 0 & 0 & 1 \\ 0 & a_{42} & a_{43} & a_{44} \end{bmatrix}$$

where

$$\begin{aligned} a_{22} &= -\frac{2}{mv}(c_{\alpha f} + C_{\alpha r}), \\ a_{23} &= \frac{2}{m}(C_{\alpha f} + C_{\alpha r}), \\ a_{24} &= -\frac{2}{mv}(\ell_f C_{\alpha f} - \ell_r C_{\alpha r}), \\ a_{42} &= -\frac{2}{vI}(\ell_f C_{\alpha f} - \ell_r C_{\alpha r}) \\ a_{43} &= \frac{2}{I}(\ell_f C_{\alpha f} - \ell_r C_{\alpha r}) \\ a_{44} &= -\frac{2}{vI}\left({\ell_f}^2 C_{\alpha f} + {\ell_r}^2 C_{\alpha r}\right). \end{aligned}$$

Authorized licensed use limited to: COLORADO STATE UNIVERSITY. Downloaded on April 16,2025 at 22:55:41 UTC from IEEE Xplore. Restrictions apply.

IPR2025-00943
Tesla EX1026 Page 2

Here y_{cg} is the lateral displacement of the center of gravity (c.g.) of the vehicle with respect to the road center-line and $\Delta\varepsilon$ is the relative yaw angle of the vehicle with respect to the road. The front wheel steering angle (δ) is the control input that is used to regulate lateral and yaw motion of the automated vehicle. Note that the road reference coordinates rotate on curves. This effect is represented as the desired yaw rate $\dot{\varepsilon}_d$ in (6a). The other variables and symbols used in the model are described in the Nomenclature section.

In implementing the lateral control system, vehicle lateral displacement can be measured by an on-board machine vision system [3], [9] or by a magnetic sensor system which measures displacement by measuring the magnetic field from discrete magnets buried every 1.2 m in the center of the road [21]. Magnetometers mounted on the car serve as sensors to measure the magnetic field. The output equation for lateral displacement is $y_1 = C_1 x$ with

$$C_1 = [1 \quad 0 \quad d_s \quad 0] \tag{7}$$

where d_s is the longitudinal distance between the magnetometer and the vehicle c.g. In addition, on-board inertial sensors such as a yaw-rate sensor and a lateral accelerometer are available and are typically used by the lateral control system. The outputs equations for these sensors are given below:

Yaw-rate sensor: $y_2 = C_2 x$ with

$$C_2 = [0 \quad 0 \quad 0 \quad 1] \tag{8}$$

and lateral accelerometer: $y_3 = C_3 x + b_{12}\delta + b_{22}\dot{\varepsilon}_d$ with

$$C_3 = [0 \quad a_{22} \quad a_{23} \quad a_{24}] \tag{9}$$

where a_{ij} and b_{ij} refer to the corresponding elements of the matrices in (6a).

C. Controller Design

From (1) and (2), it is clear that the acceleration of the jth vehicle can be controlled to any desired positive value $\ddot{x}_{j_\mathrm{des}}$ by choosing the net combustion torque to be

$$(T_{\mathrm{net}})_j = \frac{J_e}{Rh}\ddot{x}_{j_\mathrm{des}} + \left[c_a R^3 h^3 {\omega_e}^2 - R(hF_f + T_{\mathrm{br}})\right]_j. \tag{10}$$

By choosing the combustion torque to be the function described above ([7]), the acceleration of the jth vehicle becomes

$$\ddot{x}_j = \ddot{x}_{j_\mathrm{des}} \tag{11}$$

The desired acceleration $\ddot{x}_{j_\mathrm{des}}$ for each car has to be determined so that a desired constant spacing is maintained between the cars of the platoon and string stability of the platoon is ensured.

For an explanation of "string stability," see ([7], [10]) and the references therein. String stability guarantees that spacing errors do not amplify upstream from the lead car. For instance, string stability would ensure that any error in spacing between the first and second cars of the platoon does not amplify into a huge spacing error between cars 7 and 8 further down the platoon.

Swaroop *et al.* [10] have shown that both string stability and robustness can be achieved even with very small inter-vehicle spacing if feedback information from all of the following signals is used in determining the desired acceleration of each vehicle:

- acceleration of preceding car;
- the car's relative velocity with respect to preceding car;
- distance to preceding car;
- acceleration of lead car of the platoon;
- relative velocity with respect to lead car of the platoon.

A wireless communication system is used between the cars to obtain access to all of the above signals. Each car thus obtains communicated information from two other cars in the platoon—the lead car and the preceding car.

Once the desired combustion torque has been determined from (10), the desired mass of air in the intake manifold and consequently the throttle angle α can be determined by using a "multisurface" sliding mode controller, as described in [7]. The sensor measurements needed are manifold pressure and engine speed. The intake manifold temperature is assumed to be constant. If the brake actuator needs to be used for providing the desired synthetic acceleration, the desired brake torque T_{br} can be calculated from (10) by setting the net combustion torque to zero. Here we assume that the brake torque is an actuator input to the system and can be directly specified by the user.

The lateral control systems developed and experimentally implemented at California PATH include the frequency shaped linear quadratic (FSLQ) controller with preview (Peng and Tomizuka, [15]), linear controllers using "virtual look-ahead" by using front and rear magnetometers [19] and controllers designed using a nonlinear system approach (Pham *et al.* [16], Hingwe and Tomizuka [8] and Chen and Tomizuka [1]). The controllers use longitudinal velocity as a known time varying parameter and yaw-rate sensor, magnetometer and lateral accelerometer for feedback.

D. Sensors and Actuators

Having reviewed the vehicle dynamics model and the controllers, we now find that the following sensors as indicated by Table I are needed by the longitudinal and lateral control systems. The information lost due to a fault in any of these sensors is also indicated in the table.

In addition to the sensors listed above that are required by the control system, we will assume that a sensor to measure the actual front wheel steering angle is available. This is in addition to the steering angle sensor that measures the angle of the driver's steering wheel.

The steering actuator, throttle actuator and the brake actuator are the three actuators used by the control system which need to be monitored. Throttle angle, brake torque and steering angle are the corresponding actuator inputs.

III. Analytical Redundancy Using Observers

A. Overview of the Fault Diagnostic System Design Procedure

The fault diagnostic system proposed in this paper is based on the use of parity equations. A parity equation is an algebraic equation that is assumed to be satisfied in the absence of faults and sensor noise. For example, if sensor outputs are related in such a way that the variable one sensor measures can be

Authorized licensed use limited to: COLORADO STATE UNIVERSITY. Downloaded on April 16,2025 at 22:55:41 UTC from IEEE Xplore. Restrictions apply.

IPR2025-00943
Tesla EX1026 Page 3

TABLE I
COMPLETE SET OF SENSORS

SENSOR FAULT	INFORMATION LOST
STEERING ANGLE SENSOR	Steering angle
YAW-RATE SENSOR	Yaw rate
MAGNETOMETER	Lateral displacement of car with respect to magnetic markers on the road
LATERAL ACCELEROMETER	Lateral acceleration of car
RADIO	Lead and previous vehicle's velocity and acceleration
RADAR	Distance and relative velocity from preceding car
LONGITUDINAL ACCELEROMETER	Acceleration (used by following cars in the platoon)
WHEEL SPEED SENSOR	Velocity
THROTTLE ANGLE SENSOR	Throttle angle
BRAKE PRESSURE SENSOR	Brake-line pressure
MANIFOLD PRESSURE SENSOR	Intake manifold pressure
ENGINE RPM SENSOR	Engine speed

determined by the instantaneous outputs of the other sensors, then a parity equation that defines the instantaneous relation between the sensor outputs can be constructed. Parity equations can also be constructed with the use of observers. An observer based on an analytical model can be used to estimate one sensor signal from measurement of other sensor signals. If the observer is asymptotically stable, the estimation error is expected to be equal to zero in the absence of faults and this would constitute a parity equation.

As the following sections describe, the fault diagnostic system in this paper relies on the construction of residues. Each residue is used to check how well a particular parity equation is satisfied.

If three sensor signals are algebraically related so that there exist three independent parity equations relating these signals, then the three residues obtained from these parity equations can be used to determine exactly which of the three sensors is at fault (assuming that not more than one sensor becomes faulty at the same time). This fact is used in Section III-C to determine if either of the wheel speed, engine speed or range rate sensors are at fault.

Once it is ensured that the engine speed, wheel speed and range rate sensors are all operational, several reduced order observers are designed using these sensor signal measurements. These observers are used to diagnose the health of the other sensors and actuators. For example, a second order observer that utilizes engine speed measurement and commanded throttle angle as inputs is used to estimate engine manifold pressure and engine speed. A comparison of the estimated and measured engine speeds is used to determine if the throttle actuator is at fault. The estimated manifold pressure is used to determine if the manifold pressure sensor is at fault.

Section III-F describes the design of a first order observer utilizing engine speed measurement and commanded brake torque to diagnose the health of the brake actuator. Section III-G describes an observer to estimate vehicle speed using an accelerometer and magnetic markers. This observer is used to diagnose the health of the peak detection ability of the magnetometer. Section III-D describes the design of an observer that estimates inter-car spacing using magnetic markers and the difference of wheel speeds in the two cars. This is used to diagnose the health of the radar sensor. Similarly, in the case of the lateral control system, the three lateral sensors—yaw-rate sensor, lateral accelerometer and magnetometer—are used in the design of three different observers. The output estimation errors from the observers are used to uniquely identify a fault in any one of the three sensors. In addition the wheel speed sensor whose health has been previously diagnosed by the longitudinal fault diagnostics, is used to obtain vehicle speed needed by the observers for the lateral sensors. Steering wheel angle, vehicle wheel angle, and commanded steering angle are related by parity equations and used to ensure that the steering actuator and the two angle sensors are working.

From the above summary, it is clear that observer design plays a key role in the fault diagnostic system design. Since the mathematical models for the vehicle dynamics are nonlinear, it is a challenge to ensure that the observers for the system are stable, robust and can be designed to have required rates of convergence. The observer design procedure used is described in Section III-B.

Section IV integrates the parity equations and observers designed in Section III to create a systematic methodology for fault diagnostics that can uniquely identify the particular sensor or actuator that is at fault.

B. Observer Design for Nonlinear Systems

The design of exponentially stable observers for systems with nonlinear dynamics will be based on the following results from Rajamani and Cho ([17], [18]).

Given a nonlinear system

$$\dot{x} = Ax + \Phi(x, u) \tag{12a}$$

$$y = Cx \tag{12b}$$

where

1) $\Phi(x, u)$ is a Lipschitz nonlinearity with a Lipschitz constant γ, i.e.,

$$||\Phi(x, u) - \Phi(\hat{x}, u)|| \leq \gamma ||x - \hat{x}|| \quad \forall\, x, \hat{x}$$

2) A is stable and the distance to undetectability of the pair (A, C) is larger than the Lipschitz constant γ of the nonlinear function $\Phi(x, u)$

there exists a matrix L such that the estimates from the following observer:

$$\dot{\hat{x}} = A\hat{x} + \Phi(\hat{x}, u) + L(y - C\hat{x}) \tag{13}$$

converge exponentially to the states of the system defined by (12a).

Authorized licensed use limited to: COLORADO STATE UNIVERSITY. Downloaded on April 16,2025 at 22:55:41 UTC from IEEE Xplore. Restrictions apply.

An explicit analytical solution for the observer gain matrix L can be provided as follows.

Solve

$$A^{\mathrm{T}}P + PA + \gamma^2 PP + I - \frac{C^{\mathrm{T}}C}{\gamma^2} < 0 \tag{14a}$$

and then choose

$$L = \frac{P^{-1}C^{\mathrm{T}}}{2\gamma^2}. \tag{14b}$$

The distance to undetectability of the pair (A, C) ($A \in R^{n\times n}$ and $C \in R^{p\times n}$) is defined as the magnitude of the smallest perturbation $(E, F) \in C^{n\times n} \times C^{n\times p}$ that makes the pair $(A + E, C + F)$ undetectable.

$$\delta(A, C) = \inf_{(\mathbf{A+E},\mathbf{C+F})\ \mathbf{undetectable}} \left\| \begin{bmatrix} E \\ F \end{bmatrix} \right\|_2 .$$

While the distance to undetectability is not very easy to calculate numerically, it can be shown that if the distance to undetectability is larger than γ, then [18]

$$\min_{\omega} \sigma_{\min} \begin{bmatrix} j\omega I - A \\ C \end{bmatrix} > \gamma. \tag{15}$$

If (15) is satisfied, then the observer design results of (14a) and (14b) still hold and an asymptotically stable observer can be obtained.

C. Speed Sensor Redundancy

The longitudinal speed of the vehicle can be obtained by three different methods, as described in [5].

1) Wheel speed sensor
   Multiply angular wheel speed by the tire radius to obtain longitudinal velocity. It is assumed that there is no slip between the tire and the road.
2) For operation in the gears 3 and 4, the torque converter is locked. The engine speed is then directly related to the wheel speed by the gear ratio.
3) The closing rate with the preceding vehicle (relative velocity) can be obtained using the radar sensor. The speed of the preceding vehicle is obtained through radio communication. The two variables can be algebraically summed to obtain longitudinal velocity.

The following three residues are then calculated by using different combinations of the above three longitudinal velocity signals:

$\mathbf{R}_1$ = wheel speed/engine speed residual;
$\mathbf{R}_2$ = wheel speed/radar range rate residual;
$\mathbf{R}_3$ = engine speed/radar range rate residual.

Table II can then be used to detect a fault in any one of the three speed sensors.

D. Inter-Vehicle Spacing

We propose the following two methods to obtain inter-car spacing information.

TABLE II
TRUTH TABLE FOR PEED SENSOR FAULT DETECTION

Faulty Component	*Residual* R_1	*Residual* R_2	*Residual* R_3
Radar closing – rate sensor	Low	High	High
Engine speed sensor	High	Low	High
Wheel speed sensor	High	High	Low

1) Currently a radar sensor is used to measure the distance to the preceding car

$$\delta_i = x_i - x_{i-1} - \ell_{i-1} \tag{16}$$

where ℓ_{i-1} is the preceding vehicle length.

2) The following observer is proposed in this paper to obtain one more estimate of inter-car spacing. This observer uses a magnetometer measurement to count the number of magnetic markers passed by the two vehicles

$$\dot{\hat{\delta}}_i = v_i - v_{i-1} + k_s[(n_1 - n_2)L + \delta_o - \hat{\delta}_i] \tag{17}$$

where

$n_1 - n_2$ difference in the number of markers passed by the two vehicles;
L inter-marker spacing;
δ_0 initial spacing.

The estimation error using the given observer is

$$\dot{\tilde{\delta}}_i = -k_s[(n_1 - n_2)L + \delta_0 - \hat{\delta}_i]. \tag{18}$$

The variable $[(n_1 - n_2)L + \delta_o - \hat{\delta}_i]$ is equal to $\tilde{\delta}_i$ to within a resolution of L meters. The use of this variable ensures that any drift associated with integrating the velocities $v_i - v_{i-1}$ is eliminated. If the signal $v_i - v_{i-1}$ were perfect with no dc offsets, the use of the signal $[(n_1 - n_2)L + \delta_o - \hat{\delta}_i]$ would be unnecessary.

E. Throttle Actuator and Manifold Pressure Sensor Faults

In [5], two different nonlinear detection filters are proposed for throttle actuator and manifold mass flow rate fault detection. A first order detection filter is constructed so as to estimate engine speed asymptotically in the absence of throttle actuator fault. A fourth-order detection filter that estimates manifold mass flow rate along with several other variables is also proposed for fault diagnosis of the mass flow rate sensor.

We propose using one second —order nonlinear observer to estimate both the engine speed and manifold pressure utilizing commanded throttle angle and engine speed measurement as inputs. This observer

$$\dot{\hat{\omega}}_e = \frac{T_{\mathrm{net}}(\hat{\omega}_e, \hat{m}_a) - c_a R^3 h^3 \hat{\omega}_e^2 - RhF_f}{J_e} + \ell_1(\omega_e - \hat{\omega}_e) \tag{19}$$

$$\dot{\hat{m}} = \mathrm{MAX}\, TC(\alpha_{\mathrm{des}})\mathrm{PRI}(\hat{\omega}_a) - \dot{m}_{ao}(\hat{\omega}_e, \hat{m}_a) + \ell_2(\omega_e - \hat{\omega}_e) \tag{20a}$$

$$\hat{P}_m V = \hat{m}_a R_g T_m \tag{20b}$$

Authorized licensed use limited to: COLORADO STATE UNIVERSITY. Downloaded on April 16,2025 at 22:55:41 UTC from IEEE Xplore. Restrictions apply.

can be designed to be asymptotically stable in the absence of throttle actuator faults by proper choice of gains ℓ_1 and ℓ_2. Since the engine speed is physically limited, the nonlinearity ω_e^2 can be regarded as locally Lipschitz and the Lipschitz constant of $c_a R^3 h^3 \hat{\omega}_e^2$ can be calculated. The linearized system equations corressponding to (19)–(20) are

$$\begin{Bmatrix} \dot{\omega}_e \\ \dot{m}_a \end{Bmatrix} = \begin{bmatrix} 0.6 & -0.5 \\ 0.3 & 1 \end{bmatrix} \begin{Bmatrix} \omega_e \\ m_a \end{Bmatrix} + \begin{bmatrix} -0.3 \\ 0 \end{bmatrix} T_{\text{brake}} + \begin{bmatrix} 0 \\ 0.6293 \end{bmatrix} TC(\alpha) \tag{21a}$$

$$\omega_e = [1 \quad 0] \begin{Bmatrix} \omega_e \\ m_a \end{Bmatrix}. \tag{21b}$$

A throttle actuator fault will cause the residue between estimated and measured engine speeds to grow. Assuming no fault in the engine speed measurement sensor, the growth in this residue can then be used to diagnose a throttle actuator fault. If a throttle actuator fault has *not* occurred, the residue between measured and estimated manifold pressure can be used for diagnostics of the manifold pressure sensor.

F. Brake Actuator/Sensor Fault

Under the action of brakes, the throttle actuator is not used. The variable T_{net} can therefore be set to zero in (2). The following observer can then be used to estimate the engine speed under the action of the braking actuator

$$\dot{\hat{\omega}}_e = \frac{-c_a R^3 h^3 \hat{\omega}_e^2 - R(hF_f + T_{\text{br_des}})}{J_e} + \ell(\omega_e - \hat{\omega}_e). \tag{22}$$

The dynamics of the estimation error $\tilde{\omega}_e = \omega_e - \hat{\omega}_e$ are then given by

$$\dot{\tilde{\omega}}_e = -a\tilde{\omega}_e^2 - \ell\tilde{\omega} - c\mu(t) \tag{23}$$

where $a = (c_a R^3 h^3 / J_e)$, $c = R/J_e$ and $\mu(t)$ is nonzero only when there is a fault in the brake actuator. Since the engine speed can never physically exceed 4000 r/min, the nonlinearity ${\omega_e}^2$ can be regarded as locally Lipschitz. Since the observer has access to a measurement of ω_e, the gain ℓ can be chosen larger than the Lipschitz constant of ${\omega_e}^2$ in order to ensure stablity of the estimation error dynamics in the absence of faults.

G. Vehicle Speed Estimation using Accelerometers and Magnetic Markers

The following observer using the accelerometer on the car and a magnetometer measurement to count the number of magnetic markers passed by the car can be used to estimate car velocity

$$\dot{\hat{v}} = a_i + k_v \left(\frac{n_1 L}{T} - \hat{v} \right). \tag{24}$$

The estimation error using the given observer is

$$\dot{\tilde{v}} = -k_v \left(\frac{n_1 L}{T} - \hat{v} \right). \tag{25}$$

TABLE III
TRUTH TABLE FOR STEERING ANGLE/STEERING ACTUATOR FAULT DETECTION

Faulty Component	*Residual* R_{11}	*Residual* R_{12}	*Residual* R_{13}
Steering actuator	High	High	Low
Steering angle sensor	High	Low	High
Wheel angle sensor	Low	High	High

The variable $((n_1 L/T) - \hat{v})$ is equal to $\tilde{v}_i$ to within a resolution of L meters. The use of this variable ensures that any drift associated with integrating the acceleration a_i is eliminated. If the signal a_i were perfect with no dc offsets, the use of the signal $((n_1 L/T) - \hat{v})$ would be unnecessary.

H. Communication Fault

1) The car that communicates ensures that its sensors are not faulty.
2) If no communication packet is received, the information from the last packet is frozen till the next packet arrives.
3) If no packet is received for more than three consecutive cycles, a communication fault is declared.

I. Estimation of Yaw-Rate using Magnetometer

If we assume that the lateral magnetometer sensor is working, the yaw-rate of the car can be estimated by an observer using this sensor. The observability matrix

$$\begin{bmatrix} C_1^{\text{T}} & (C_1 A)^{\text{T}} & \left(C_1 A^2\right)^{\text{T}} & \left(C_1 A^3\right)^{\text{T}} \end{bmatrix}^{\text{T}} \tag{26}$$

has rank 4 which makes the states completely observable. The residue

$$R_{14} = C_2 \hat{x} - y_2 \tag{27}$$

can then be used to determine if the yaw-rate sensor is faulty.

J. Estimation of Lateral Acceleration

If we assume that the magnetometer sensor is working and that the steering angle sensor is not faulty, the lateral acceleration of the car can be estimated by an observer using these two sensors. The observability matrix of (26) has rank 4 which makes the states completely observable. The residue

$$R_{15} = C_3 \hat{x} - y_3 \tag{28}$$

can then be used to determine if the lateral acceleration sensor is faulty.

K. Estimation of Lateral Displacement

If we assume that the lateral acceleration and yaw-rate sensors are working, one could try and estimate lateral displacement, usually measured by the magnetometer. However, the observability matrix

$$\begin{bmatrix} C_2^{\text{T}} & (C_3)^{\text{T}} & (C_3 A)^{\text{T}} & (C_3 A)^{\text{T}} & \cdots \end{bmatrix}^{\text{T}} \tag{29}$$

has a rank of only 3 which means the complete state is not observable with these measurements!

Authorized licensed use limited to: COLORADO STATE UNIVERSITY. Downloaded on April 16,2025 at 22:55:41 UTC from IEEE Xplore. Restrictions apply.

TABLE IV
BANK OF SIGNALS FOR FAULT DIAGNOSTICS

SIGNAL	DESCRIPTION	SENSOR/ OBSERVER
$z_1 = h\omega_w$	vehicle speed	wheel speed sensor
$z_2 = R\,h\omega_e$	engine speed	engine speed and gear ratio sensors
$z_3 = x_{i-1} - x_i$	distance to preceding car (range)	radar range signal
$z_4 = v_{i-1} - v_i$	relative velocity of preceding car	radar range rate signal
$z_5 = v_{i-1}$	velocity of preceding car	communication
$z_6 = \omega_e$	engine speed	engine speed sensor
$z_7 = P_m$	pressure of air in manifold	mass flow rate sensor
$z_8 = a_i$	longitudinal acceleration	longitudinal accelerometer
$z_9 = a_{i-1}$	longitudinal acceleration of preceding car	communication
$z_{10} = \hat{\omega}_e$	estimated engine speed	observer of eqns. (19) -(20)
$z_{11} = \hat{P}_m$	estimated pressure in manifold	observer of eqns. (19) - (20)
$z_{12} = \alpha_c$	commanded throttle angle	calculated by longitudinal controller
$z_{13} = \alpha$	throttle angle	throttle angle sensor
$z_{14} = T_{br_com}$	commanded brake torque	calculated by longitudinal controller
$z_{15} = \hat{\delta}\ i$	estimated distance to preceding car	observer of eqn. (17)
$z_{16} = \hat{v}_i$	estimated velocity	observer of eqn. (24)
$z_{17} = a_{syn}$	synthetic acceleration	calculated by longitudinal controller
$z_{18} = \omega_{e_br}$	Estimated engine speed during braking	observer of eqn. (22)
$z_{19} = y_s$	Lateral position from magnetic marker	magnetometer
$z_{20} = \Delta\dot{\varepsilon}$	Yaw rate	yaw-rate sensor
$z_{21} = \ddot{y}_{cg}$	Lateral acceleration	lateral accelerometer
$z_{22} = \hat{y}_s$	Estimated lateral displacement	observer of section 3.10
$z_{23} = \Delta\hat{\dot{\varepsilon}}$	Estimated yaw rate	observer of section 3.8
$z_{24} = \hat{\ddot{y}}_{cg}$	Estimated lateral acceleration	observer of section 3.9
$z_{25} = \delta$	Steering angle	steering angle encoder
$z_{26} = \delta_{des}$	Desired steering angle	calculated by lateral controller
$z_{27} = \delta_w$	Measured vehicle wheel angle	vehicle wheel angle sensor

The partial state-vector with dynamics defined by

$$\frac{d}{dt}\begin{Bmatrix}\dot{y}_{\rm cg}\\ \Delta\varepsilon\\ \Delta\dot{\varepsilon}\end{Bmatrix} = \begin{bmatrix}a_{22} & a_{23} & a_{24}\\ 0 & 0 & 1\\ a_{42} & a_{43} & a_{44}\end{bmatrix}\begin{Bmatrix}\dot{y}_{\rm cg}\\ \Delta\varepsilon\\ \Delta\dot{\varepsilon}\end{Bmatrix} + \begin{bmatrix}b_{22}\\ b_{23}\\ b_{24}\end{bmatrix}\dot{\varepsilon}_d + \begin{bmatrix}b_{12}\\ b_{13}\\ b_{14}\end{bmatrix}\delta \tag{30}$$

is, however, completely observable from these two outputs. This means that while $y_{\rm cg}$ is not observable, $\dot{y}_{\rm cg}$ can be estimated from the lateral accelerometer and yaw-rate sensor. If the initial condition $y_{\rm cg}(0)$ is known, then $y_{\rm cg}$ can be estimated as follows:

$$\hat{y}_{\rm cg}(t) = \int \hat{\dot{y}}_{\rm cg}dt + y_{\rm cg}(0). \tag{31}$$

The residue

$$R_{16} = \hat{y}_{\rm cg}(t) - y_{\rm cg}(t) \tag{32}$$

can then be used to determine if the magnetometer sensor is faulty.

L. Fault Diagnostics of Steering Angle Sensor/Steering Actuator

If we assume that the steering wheel angle and the vehicle wheel angle are both measured, then the two sensors are related by a scaling factor. The steering wheel angle, vehicle wheel angle and commanded steering angle are related by three independent parity equations. The following three residues are then calculated by using different combinations of the above three signals.

$\mathbf{R}_{11}$ = commanded steering angle/measured steering angle.

Authorized licensed use limited to: COLORADO STATE UNIVERSITY. Downloaded on April 16,2025 at 22:55:41 UTC from IEEE Xplore. Restrictions apply.

TABLE V
CALCULATION OF RESIDUES

RESIDUES	SENSORS/ ACTUATORS INVOLVED
$R_1 = z_1 - z_2$	wheel speed sensor, engine speed sensor
$R_2 = z_5 - z_4 - z_1$	radar range rate sensor, wheel speed sensor, communication
$R_3 = z_5 - z_4 - z_2$	radar range rate sensor, engine speed sensor, communication
$R_4 = z_3 - z_{15}$	radar range sensor, wheel speed sensor, magnetometer, communication
$R_5 = z_{17} - z_8$	longitudinal accelerometer
$R_6 = z_{16} - z_1$	long. accelerometer, magnetometers, wheel speed sensor
$R_7 = z_{10} - z_6$	throttle actuator, engine speed
$R_8 = z_{12} - z_{13}$	throttle angle sensor, throttle actuator
$R_9 = z_{11} - z_7$	pressure of air in manifold sensor, throttle actuator, engine speed sensor
$R_{10} = z_{18} - z_6$	brake actuator, engine speed
$R_{11} = z_{25} - z_{26}$	steering angle sensor, steering actuator
$R_{12} = z_{26} - z_{27}$	vehicle wheel angle sensor, steering actuator
$R_{13} = z_{25} - z_{27}$	steering angle sensor, wheel angle sensor
$R_{14} = z_{20} - z_{23}$	yaw-rate sensor, magnetometer, steering angle sensor, wheel speed sensor
$R_{15} = z_{21} - z_{24}$	magnetometer, steering angle sensor lateral accelerometer, wheel speed sensor
$R_{16} = z_{19} - z_{22}$	magnetometer, yaw-rate sensor, lateral accelerometer, steering angle sensor, wheel speed sensor

TABLE VI
BEHAVIOR OF RESIDUES UNDER SENSOR/ACTUATOR FAULTS

FAULTY SENSOR/ ACTUATOR	R_1	R_2	R_3	R_4	R_5	R_6	R_7	R_8	R_9	R_{10}	R_{11}	R_{12}	R_{13}	R_{14}	R_{15}	R_{16}
wheel speed sensor	H	H	L	H	L	H	L	L	L	L	L	L	L	H	H	H
engine speed sensor	H	L	H	L	L	L	H	L	H	H	L	L	L	L	L	L
radar range rate sensor	L	H	H	L	L	L	L	L	L	L	L	L	L	L	L	L
radar range sensor	L	L	L	H	L	L	L	L	L	L	L	L	L	L	L	L
long. Accelerometer	L	L	L	L	H	H	L	L	L	L	L	L	L	L	L	L
magnetometer (longitudinal)	L	L	L	H	L	H	L	L	L	L	L	L	L	H	H	H
throttle actuator	L	L	L	L	L	L	H	H	H	L	L	L	L	L	L	L
throttle angle sensor	L	L	L	L	L	L	L	H	L	L	L	L	L	L	L	L
manifold pressure sensor	L	L	L	L	L	L	L	L	H	L	L	L	L	L	L	L
brake actuator	L	L	L	L	L	L	L	L	L	H	L	L	L	L	L	L
steering angle sensor	L	L	L	L	L	L	L	L	L	L	H	L	H	H	H	H
Magnetometer (lateral position sensing)	L	L	L	H	L	H	L	L	L	L	L	L	L	H	H	H
yaw-rate sensor	L	L	L	L	L	L	L	L	L	L	L	L	L	H	L	H
lateral accelerometer	L	L	L	L	L	L	L	L	L	L	L	L	L	L	H	H
steering actuator	L	L	L	L	L	L	L	L	L	L	H	H	L	L	L	L
wheel angle sensor	L	L	L	L	L	L	L	L	L	L	L	H	H	L	L	L

$\mathbf{R}_{12}$ = commanded steering angle/measured vehicle wheel angle.

$\mathbf{R}_{13}$ = measured steering wheel angle/measured vehicle wheel angle.

Table III can then be used to detect a fault in any one of the following three components : steering actuator, steering angle sensor, vehicle wheel angle sensor.

IV. A SYSTEM FOR AUTOMATED FAULT DIAGNOSTICS

Table IV summarizes 27 different signals to be used in the fault detection and identification scheme. Some of the signals are directly measured while others are estimates obtained from the observers discussed in the previous section. Table V summarizes 16 different residues calculated using combinations of the signals from Table IV. It is assumed that the failure of any sensor

Authorized licensed use limited to: COLORADO STATE UNIVERSITY. Downloaded on April 16,2025 at 22:55:41 UTC from IEEE Xplore. Restrictions apply.

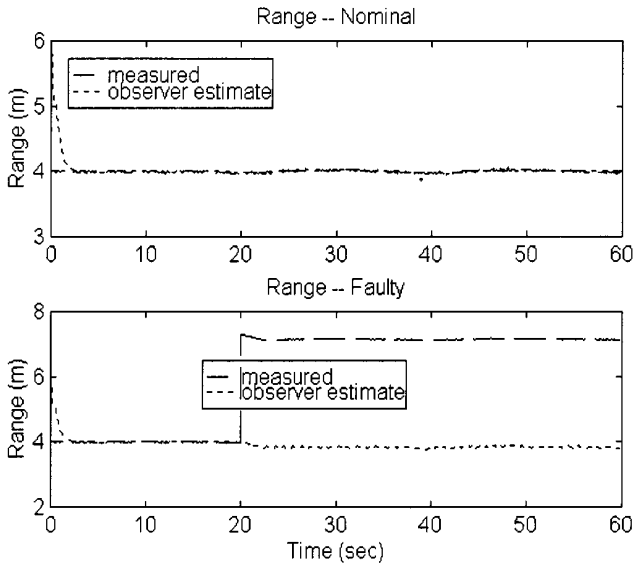

Fig. 1. Inter-car spacing observer in the absence and presence of faults.

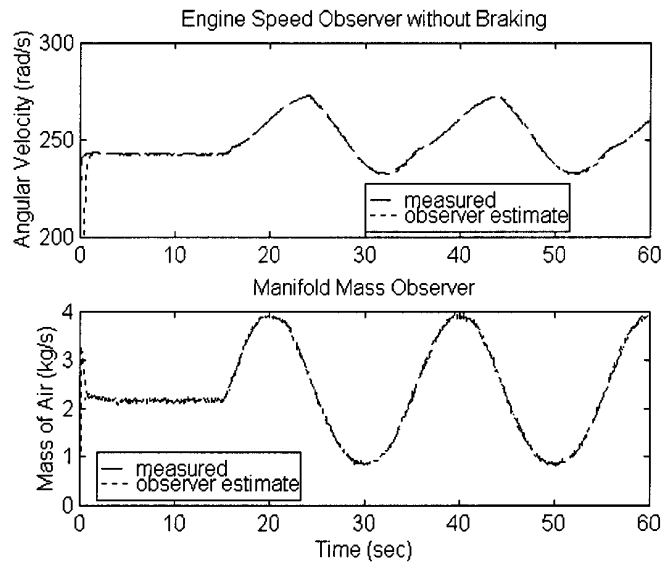

Fig. 2. Engine speed observer of (11) and (12) in the absence of faults.

would cause a residue computed by subtracting this sensor measurement from an estimate of its signal using other measurements to grow.

By processing the above 16 residues, it is possible to identify a fault in any of the sensors or actuators. Table VI shows how a fault in any one of the sensors or actuators causes a unique combination of residues to grow. Please note that the fault diagnostic is not designed to handle simultaneous multiple sensor or actuator failures.

To detect and identify faults, the algorithm on the following page can be used. The algorithm has been obtained from Table VI and is a systematic method of using Table VI to successively check for faults in each of the sensors and actuators.

V. Simulation Results

The fault detection system designed in the previous sections was simulated to test its performance with a more realistic vehicle model incorporating a torque converter, wheel slip, tire radius variation, sensor noise, etc. Details of the full vehicle simulation model are available in [15]. The noise levels assumed for the sensor measurements are shown in Table I of Section II and are realistic estimates based on experimental measurement. The marker spacing was assumed to be 1 m.

For the simulation, a three-car platoon was assumed to be traveling with a spacing of 4 m at a speed of 70 mi/h. At time $t = 15$ s, the lead car begins the following velocity maneuver:

$$v_{\text{des}} = 70 + 4.0[1 - \cos 20\pi(t - 15)]. \tag{33}$$

Fig. 1 shows the convergence of the inter-car spacing observer and its ability to track the actual radar measurement in the presence of noise and 1–m marker spacing.

Fig. 2 shows the performance of the second-order nonlinear observer of (11) and (12). The engine speed and mass flow rate of air in the manifold are estimated well by the observer. Fig. 3 shows the performance of the engine speed observer during braking (of (13)) and the performance of the velocity observer of (24).

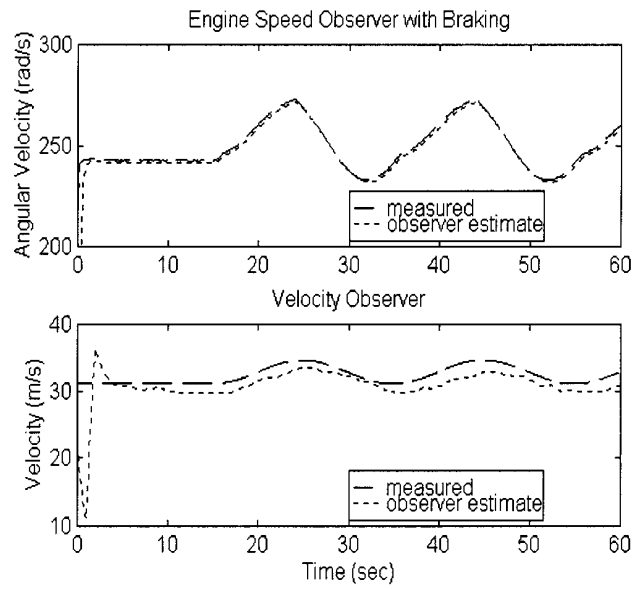

Fig. 3. Engine speed observer during braking and vehicle velocity observer.

Fig. 4 shows the performance of the lateral control system using a nonlinear "back-stepping" controller described in [1]. The GM Buick being simulated negotiates a curve of radius of curvature 1500 m at a speed of 30 m/s. The vehicle enters the trapezoidal curve at $t = 4.5$ s and leaves the trapeziodal curve at $t = 8.5$ s. The lateral displacement of the car is maintained to within ± 5 cms while the yaw angle remains within ± 0.5 degrees. The performance of the yaw rate observer of Section III-I in which the magnetometer is used to estimate yaw rate is shown in Fig. 5. Starting from an arbitrary initial yaw-rate of 6 deg/s, the observer converges to the measured yaw-rate sensor and performs well in the presence of ± 2 cms cm of noise in the magnetometer.

Authorized licensed use limited to: COLORADO STATE UNIVERSITY. Downloaded on April 16,2025 at 22:55:41 UTC from IEEE Xplore. Restrictions apply.

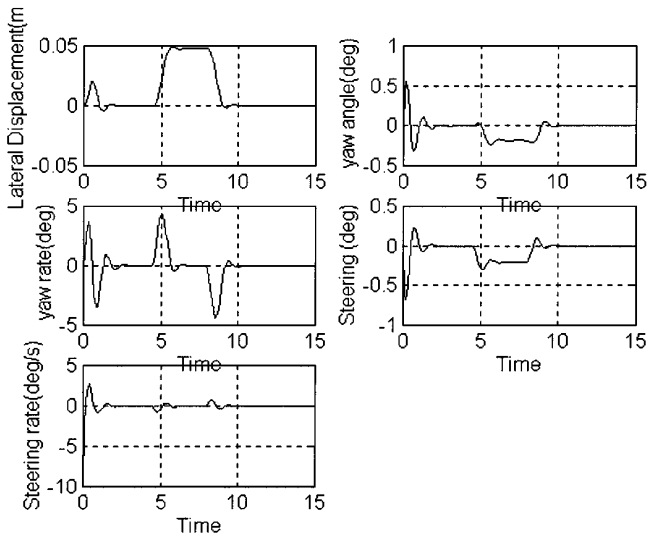

Fig. 4. Performance of the lateral control system.

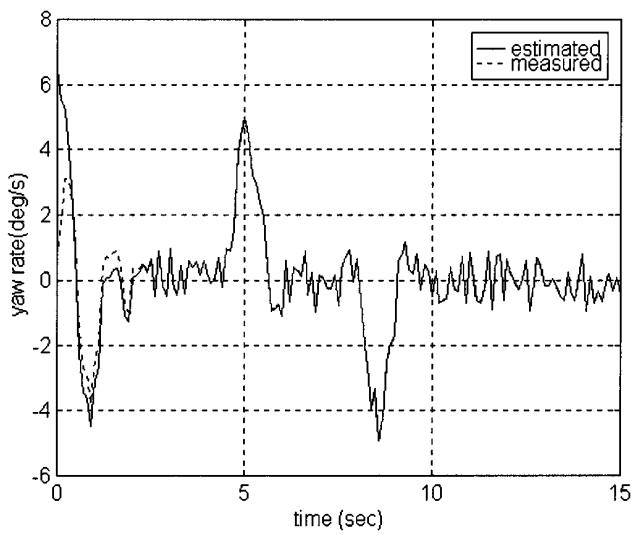

Fig. 5. Performance of the yaw-rate observer of sec. 3.9.

In the presence of a radar fault, the inter-car spacing observer diverges distinctly from the measured value, as shown in the lower portion of Fig. 1. Here a fault in the radar was assumed to cause it to read a constant value of 7 m. The observer estimate stays at a value of 4 m, thus ensuring that the residue from the radar measurement is sufficiently big to identify the fault. Fig. 6 shows the values of all the 16 residues of Table VI during the radar fault. We see that only residue 4 is high which clearly indicates from Table V that the radar sensor is the faulty component.

VI. Experimental Results

This section presents experimental results on the use of the magnetic observer of (17) and (18). The magnetic observer was implemented on the automated cars in the August 1997 NAHSC (National Automated Highway System Consortium) demonstration. The observer was used both to detect faults in the radar range sensor and also to replace the radar in the closed-loop controller in the event of a radar fault.

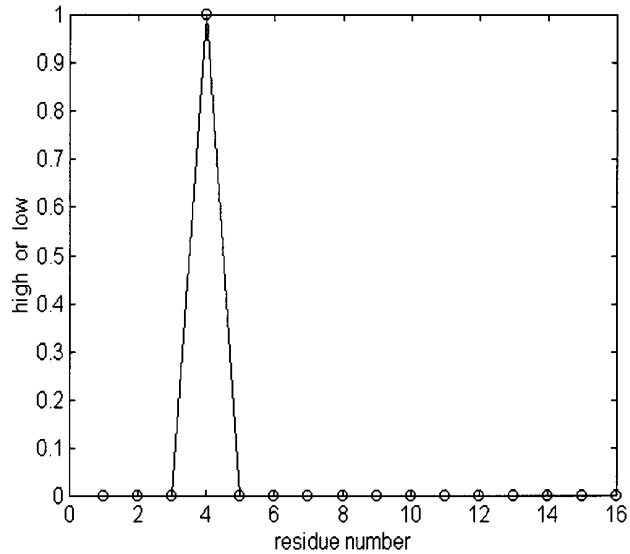

Fig. 6. Values of the different residues of Table VI during a radar sensor fault.

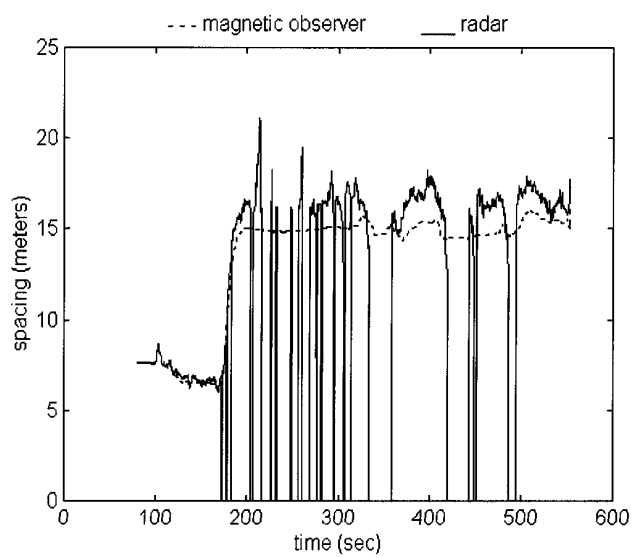

Fig. 7. Experimental results on use of magnetic observer for radar faults.

The August 1997 NAHSC demonstration showcased a platoon of eight cars traveling together at small inter-vehicle spacing forming a platoon. The demonstration was held in San Diego using a 7.6 mile two-lane highway that had been equipped with magnets installed in the centers of both lanes. The magnets served as reference markers that were used by the automated steering control system to keep each car centered in its lane. Visitors were given passenger rides in the platoon vehicles which operated continuously for several hours a day for three weeks. The presence of eight cars in a platoon with small inter-car spacing meant that any faults had to be handled by an automated fault management system. Depending on human alertness and human take-over was impossible in this scenario.

The magnetic observer played a very important role in ensuring safe automated operation during the demonstration. Radar range sensor faults were detected and automatically replaced by the magnetic observer on several occasions during the platoon runs.

Authorized licensed use limited to: COLORADO STATE UNIVERSITY. Downloaded on April 16,2025 at 22:55:41 UTC from IEEE Xplore. Restrictions apply.

The residue between radar range and the spacing estimated by the magnetic observer was processed using a low-pass filter with a bandwidth of 1 Hz. The failure detection threshold was set to 3 m.

The following plot (Fig. 7) is a good illustration of the ability of the magnetic observer to replace the radar range sensor. To allow range measurement, a rectangular opening had been cut into the front grill of each car. The radar was located behind this grill and below the hood of each car. In the following test run, a mis-orientation of the grill mounting caused the radar to fail repeatedly on the fifth car in the platoon. The readings of the radar jump from zero to the correct spacing value many times during the run.

The magnetic observer worked well throughout this run and provided a fairly accurate estimate of inter-car spacing. The fault detection system was triggered due to the 6–m difference in the actual and estimated values of range. In response to the radar fault, the spacing between cars 5 and 4 was increased to 15 m by the fault management system. The reminder of the run continued at this larger spacing. The closed-loop controller using the magnetic observer to replace the radar in the calculation of synthetic acceleration was able to provide excellent ride with a spacing variation of less than 1.3 m. The maximum errors in spacing occurred in the presence of uphill and downhill grades.

VII. Conclusion

The diagnostic system developed in this paper provides a methodology to continuously monitor all the sensors and actuators of the longitudinal and lateral controllers so as to ensure their health. The fault diagnostic system was shown to work well when simulated with a detailed vehicle model incorporating realistic unmodeled dynamics. Experimental results using the magnetic observer to detect radar faults and replace the radar sensor were shown to work extremely effectively.

Experimental implementation of the entire fault diagnostic system on the platooning vehicles at PATH is planned for the near future. The development of a complete fault handling system, however, remains a task for future research. Based on the type of fault, strategies that ensure continued safe operation of the platoon by initiating degraded modes of operation (like autonomous control or a safe deceleration to a stop) are needed.

References

[1] C. Chen and M. Tomizuka, "Vehicle lateral control on automated highways: A backstepping approach," in *Proc. IEEE Conf. Decision Contr.*, Dec. 1997.

[2] D. Cho and J. K. Hedrick, "Automotive powertrain modeling for control," *ASME Trans. Dyn. Syst., Measurement, Contr.*, vol. 111, no. 4, Dec. 1989.

[3] E. D. Dickmanns and V. Graefe, "Applications of dynamic monocular machine vision," *Machine Vision Applicat.*, vol. 1, pp. 241–261, 1988.

[4] R. K. Douglas and D. L. Speyer *et al.*, "Fault detection and identification with application to advanced vehicle control systems," California PATH Research, UCB-ITS-PRR-95–26, 1995.

[5] V. Garg, "Fault detection in nonlinear systems: An application to automated highway systems," Ph.D. dissertation, Univ. California, Berkeley, 1995.

[6] V. Garg and J. K. Hedrick, "Fault detection filters for a class of nonlinear systems," in *Proc. 1995 Amer. Contr. Conf.*, June 1995, pp. 1647–1651.

[7] J. K. Hedrick, D. McMahon, V. K. Narendran, and D. Swaroop, "Longitudinal vehicle controller design for IVHS systems," in *Proc. 1991 Amer. Contr. Conf.*, vol. 3, June 1991, pp. 3107–3112.

[8] P. Hingwe and M. Tomizuka, "Two alternative approaches to the design of lateral controllers for commuter buses based on sliding mode control," in Proc. 1995 ASME Int. Mech. Eng. Congr. Exposition.

[9] Q. T. Luong, J. Weber, D. Koller, and J. Malik, "An integrated stereo-based approach to automatic vehicle guidance," in *Proc. 5th ICCV*, 1995.

[10] D. Swaroop, J. K. Hedrick, C. C. Chien, and P. Ioannou, "A comparison of spacing and headway control laws for automatically controlled vehicles," *Veh. Syst. Dyn.*, vol. 23, no. 8, pp. 597–625, 1994.

[11] M. Tomizuka and J. K. Hedrick, "Automated vehicle control for IVHS systems," in *Proc. IFAC Conf.*, Sydney, Australia, 1993.

[12] S. Patwardhan and M. Tomizuka, "Robust failure detection in lateral control for IVHS," in *Proc. 1992 Amer. Contr. Conf.*, June 1992.

[13] ——, "Feedforward controller design using nonlinear model inversion for automobile tire burst," in *Trans. Syst. Amer. Soc. Mech. Eng., Dyn. Syst. Contr. Division (Publication) DSC*. New York: ASME, 1994, vol. 54, pp. 259–264.

[14] S. Patwardhan, H. S. Tan, and J. Guldner, "A general framework for automatic steering control system analysis," in *Proc. Amer. Contr. Conf.*, 1997, pp. 1598–1602.

[15] H. Peng and M. Tomizuka, "Preview control for vehicle lateral guidance in highway automation," *ASME J. Dyn. Syst., Measurement, Contr.*, vol. 115, no. 4, pp. 678–686, 1993.

[16] H. Pham, J. K. Hedrick, and M. Tomizuka, "Combined lateral and longitudinal control of vehicles for IVHS," in *Proc. 1994 Amer. Contr. Conf.*, vol. 2, Baltimore, MD, 1994, pp. 1205–1206.

[17] R. Rajamani, "Observer Design for Lipschitz Nonlinear Systems," *IEEE Trans. Automat. Contr.*, vol. 43, pp. 397–401, Mar. 1998.

[18] R. Rajamani and Y. M. Cho, "Existence and design of observers for nonlinear systems: Relation to distance to unobservability," *Int. J. Contr.*, vol. 69, no. 5, pp. 717–730, May 1998.

[19] H. S. Tan, J. Guldner, C. Chen, and S. Patwardhan, "Changing lanes on automated highways with look-down reference systems," in *Proc. 1998 IFAC Wkshp. Advances Automotive Contr.*, pp. 69–74.

[20] J. E. White and J. L. Speyer, "Detection filter design: spectral theory and algorithms," *IEEE Trans. Automat. Contr.*, vol. 32, pp. 593–603, 1987.

[21] W. Zhang and R. E. Parsons, "An intelligent roadway reference system for vehicle lateral guidance/control," in *Proc. Amer. Contr. Conf.*, San Diego, CA, 1990, pp. 281–286.

Rajesh Rajamani (M'94) received the M.S. and Ph.D. degrees from the University of California, Berkeley, in 1991 and 1993 respectively, and the B.Tech degree from the Indian Institute of Technology, Madras in 1989.

After receiving the Ph.D. degree, he worked as a Research Engineer at United Technologies Research Center (UTRC) for three years. From August 1996 to August 1998, he worked at California PATH, University of California, Berkeley, leading the research team on longitudinal control systems for the Automated Highway Systems Program. He joined the University of Minnesota in September 1998 and is Nelson Assistant Professor in the Department of Mechanical Engineering. His active research interests include control design and state estimation for nonlinear systems, fault diagnostics, intelligent transportation systems, vibration control and active noise control. He has authored more than 35 refereed publications and received two patents.

He is a recipient of the CAREER award from the National Science Foundation, the Distinguished Service Team Award from the University of California, Berkeley and the Outstanding Achievement of the Year Award from UTRC in 1995 for his work on Active Magnetic Guidance of Elevators

Adam S. Howell recieved the B.Sc. degree in aerospace engineering from the University of Maryland, College Park, in 1996. He is currently pursuing the Ph.D. degree in mechanical engineering at the University of California, Berkeley.

His professional interests include nonlinear systems and automated control.

Chieh Chen received the B.S. degree from the Department of Mechanical Engineering, National Taiwan University, Taiwan, in 1990 and the M.S. and Ph.D. degrees from the Department of Mechanical Engineering, University of California, Berkeley, in 1995 and 1996, respectively.

He is currently an Assistant Professor in the Department of Mechanical Engineering, National Chiao-Tung University, Taiwan. His research interests include vehicle control, real-time system design, and automation of semiconductor manufacturing equipment.

Authorized licensed use limited to: COLORADO STATE UNIVERSITY. Downloaded on April 16,2025 at 22:55:41 UTC from IEEE Xplore. Restrictions apply.

J. Karl Hedrick received the B.S. degree from the University of Michigan, Ann Arbor, in 1966, and the M.S. and Ph.D. degrees from Stanford University, Stanford, CA, in 1970 and 1971, respectively.

He was a Professor of Mechanical Engineering at the Massachusetts Institute of Technology, Cambridge, from 1974 to 1988, where he served as Director of the Vehicle Dynamics Laboratory. He is currently the James Marshall Wells Professor and Chairman of Mechanical Engineering at the University of California (UC), Berkeley. He is also the Director of the University of California PATH Research Center, a multidisciplinary research program located at the Richmond Field Station. PATH conducts research in a variety of advanced transportation areas including advanced vehicle control systems, advanced traffic management and information systems and technology leading to an automated highway system. He teaches graduate and undergraduate courses in automatic control theory and vehicle dynamics. His research has concentrated on the development of advanced control theory and on its application to a broad variety of transportation systems including automated highway systems, collision warning systems, collision avoidance systems, and adaptive cruise control systems. His work has also included brake control and electronic suspension systems. The active suspension laboratory at UC Berkeley is the only full scale, half car test facility in the United States. He has also worked in the powertrain control area including engine and transmission control. He has offered short courses on active and semiactive suspensions, nonlinear control theory and VHS in the United States and in Europe.

Dr. Hedrick has served on many national committees including the Transportation Research Board, the American National Standards Institute, ISO (International Standards Organization) and the NCHRP (National Cooperative Highway Research Program). He is currently a member of the Board of Directors and is Vice President of the International Association of Vehicle System Dynamics (IAVSD) and is the editor of the Vehicle Systems Dynamics Journal. He is a Fellow of ASME where he has served as Chairman of the Dynamic Systems and Controls Division and as Chairman of the Honors Committee. He is also a member of SAE.

Masayoshi Tomizuka (M'86–SM'95–F'97) was born in Tokyo, Japan, in 1946. He received the B.S. and M.S. degrees in mechanical engineering from Keio University, Tokyo, and the Ph.D. degree in mechanical engineering from the Massachusetts Institute of Technology, Cambridge, in February 1974.

In 1974, he joined the faculty of the Department of Mechanical Engineering at the University of California (UC), Berkeley, where he currently holds the Cheryl and John Neerhout, Jr., Distinguished Professorship Chair. At UC, he teaches courses in dynamic systems and controls. His current research interests are optimal and adaptive control, digital control, signal processing, motion control, and control problems related to robotics, machining, manufacturing, information storage devices and vehicles. He has served as a consultant to various organizations, including Lawrence Berkeley Laboratory, General Electric, General Motors, and United Technologies. He was Editor-in-Chief of the IEEE/ASME TRANSACTIONS ON MECHATRONICS from 1997 to 1999.

Dr. Tomizuka served as Technical Editor of the *ASME Journal of Dynamic Systems, Measurement and Control* from 1988 to 1993, and an Associate Editor of *Automatica*. He currently serves as an Associate Editor of the *European Journal of Control*. He was General Chairman of the 1995 American Control Conference, and served as President of the American Automatic Control Council from 1998 to 1999. He is a Fellow of the ASME, the Institute of Electric and Electronics Engineers (IEEE) and the Society of Manufacturing Engineers. He is the recipient of the J-DSMC Best Paper Award (1995), the DSCD Outstanding investigator Award (1996) and the Charles Russ Richards Memorial Award (ASME, 1997). The Charles Russ Richards Memorial Award, established in 1944, is given to an engineering graduate who demonstrates outstanding achievement in mechanical engineering 20 years or more following graduation.

Authorized licensed use limited to: COLORADO STATE UNIVERSITY. Downloaded on April 16,2025 at 22:55:41 UTC from IEEE Xplore. Restrictions apply.